Channel Measurement and Markov Modelling of an Urban Free-Space Optical Link

Ayman Mostafa, *Student Member, IEEE,* and Steve Hranilovic, *Senior Member, IEEE*

Abstract

Free-space optical (FSO) communication links provide high data rates, however, their reliability is heavily dependent on weather conditions. This paper presents our experimental, urban 1.87-km FSO link based on a customized commercial system and develops a library of channel measurements in clear and light rain weather conditions. A channel model for the link is proposed and experimentally quantified. Channel measurements are obtained by modulating a 60-mW laser source. At the receiver, a 2-GSa/s data converter is used and 16 fast-Fourier transform (FFT) cores are implemented in hardware to improve noise immunity. The resulting signal-to-noise ratio (SNR) of the channel samples is around 40 dB under clear weather conditions. Fitting with the log-normal, gamma-gamma, and Erlang distributions are presented and the scintillation index and coherence time are measured. A computationally-efficient finite-state Markov chain is derived for the channel to model both distribution and autocorrelation of the fading and is verified by the measurements. The Markov models and channel measurements in a variety of atmospheric conditions are available for download to permit easy verification of communication algorithms on this urban FSO channel.

I. INTRODUCTION

FREE-space optical (FSO) communication links are a potential solution to the last-mile problem since they combine the flexibility of RF networks and the high data rates of optical links. However, FSO communications are adversely affected by weather conditions such as fog, rain, and snow. Even under clear sky conditions, the non-homogeneity in the atmospheric structure caused by spatial and temporal temperature gradients causes random variations in the refractive index at optical wavelengths. Such non-homogeneity induces fluctuations of the signal intensity at the receiver termed as *scintillation* [1].

In order to characterize the terrestrial FSO communication link, many experimental investigations have been done, starting from early astronomical studies [2]. More recently, focus has been placed on the development of communication channel models based on experimental measurements. In [3], a 1.5-km link operating at 1550 nm is used to estimate fading distribution for a variety of receiver aperture sizes. The fitting parameters for log-normal and gamma-gamma fading distributions are compared between the analytical model and experimental data as a function of receiver diameter. All measurements were done using an unmodulated continuous-wave source only 2.1 m above the ground and irradiance measurements made at a rate of 10 kHz in clear weather. The noise was not directly estimated, but rather, an estimate of its mean is removed from all measured samples. Channel measurements on a 1550-nm, 12-km FSO system are reported in [4] to develop estimates of parameters of fading distributions. The transmitter is an unmodulated continuous-wave source and

received irradiance were sampled at 10 kHz and noise statistics are measured. Under the assumption of known noise statistics, they develop estimators for parameters of log-normal and gamma-gamma fading distributions considering fading and noise jointly. In [5], channel measurements of attenuation on a 1-km FSO link operating at 1550 nm are reported during a rain event. Although measurement data and atmospheric data are provided, no channel model is presented. A recent work [6] presents measurement results of a 1-km FSO link at 785 nm. The received photocurrent is sampled at 10 kHz for 3-sec intervals. The key contribution of the paper is the development of a Butterworth spectral fit to model the autocorrelation of the atmospheric fading model. The fitting is parameterized by temperature and rain level to give a family of spectra. A good fit in spectra is presented over a wide range of conditions, however, for convenience, the fading is modelled as being gamma distributed and not with more accepted log-normal or gamma-gamma models. In [7], pulses with a frequency of 6 MHz are transmitted for channel measurements over a 2.7-km FSO link. The received samples are bandpass filtered, rectified, and averaged to represent the received optical intensity. Although this process adds more complexity, a key advantage is attained by transmitting away from the DC region with possible coupling issues. The work presents plots of channel scintillation and attenuation but does not provide a comprehensive model for the channel.

This paper presents measurements of a 1.87-km FSO link in an urban environment. Unlike previous work which was done with laboratory equipment or for relatively short periods of time, our measurement system uses customized commercial FSO terminals coupled to a high-speed digitizing system which is able to record continuously. The digitization system uses 2-GSa/s data converters and high-speed FPGAs to collect and filter the incoming samples to improve SNR. After processing, the effective sampling rate is over 100 kHz for a continuous period of nearly 9 hours. An initial library of channel measurements is developed in clear and light rain weather conditions. This library is open for download [8] and will permit more realistic verification of communication algorithms on a commercial urban FSO channel. This work is the initial step in an ongoing campaign of channel measurement in different weather conditions which will be provided to the research community. In addition, a simple Markov model is developed to jointly represent the channel fading distribution and autocorrelation. With a small number of states, it is possible to generate long sequences of fading amplitudes which are close to measurements. Thus, this model will allow for simulation studies of FSO systems without resorting to coarse modelling assumptions of slow, block-independent fading.

Section II presents details of the experiment while Sec. III presents measurements and a channel model for the FSO transceivers. In Section IV, the procedure and measurement results are reported at different time scales and estimates of the fading distribution and coherence time are obtained. In addition, fitting with the log-normal, gamma-gamma, and Erlang distributions are presented. Section V gives a finite-state Markov chain model for the channel which is compared to measured results. Finally, concluding remarks are given in Section VI.

II. EXPERIMENTAL DETAILS

Given that the objective of this study is a long-term channel measurement in a Canadian environment, the basis of our measurement setup is a commercial FSO terminal, the *SONAbeam*™-1250-M [9]. This unit was jointly customized with the manufacturer to permit analog transmission and reception functions in addition to the standard digital operation. In addition, two *Triton*™-V5-VXS digitizer boards [10] are employed on each end of the link.
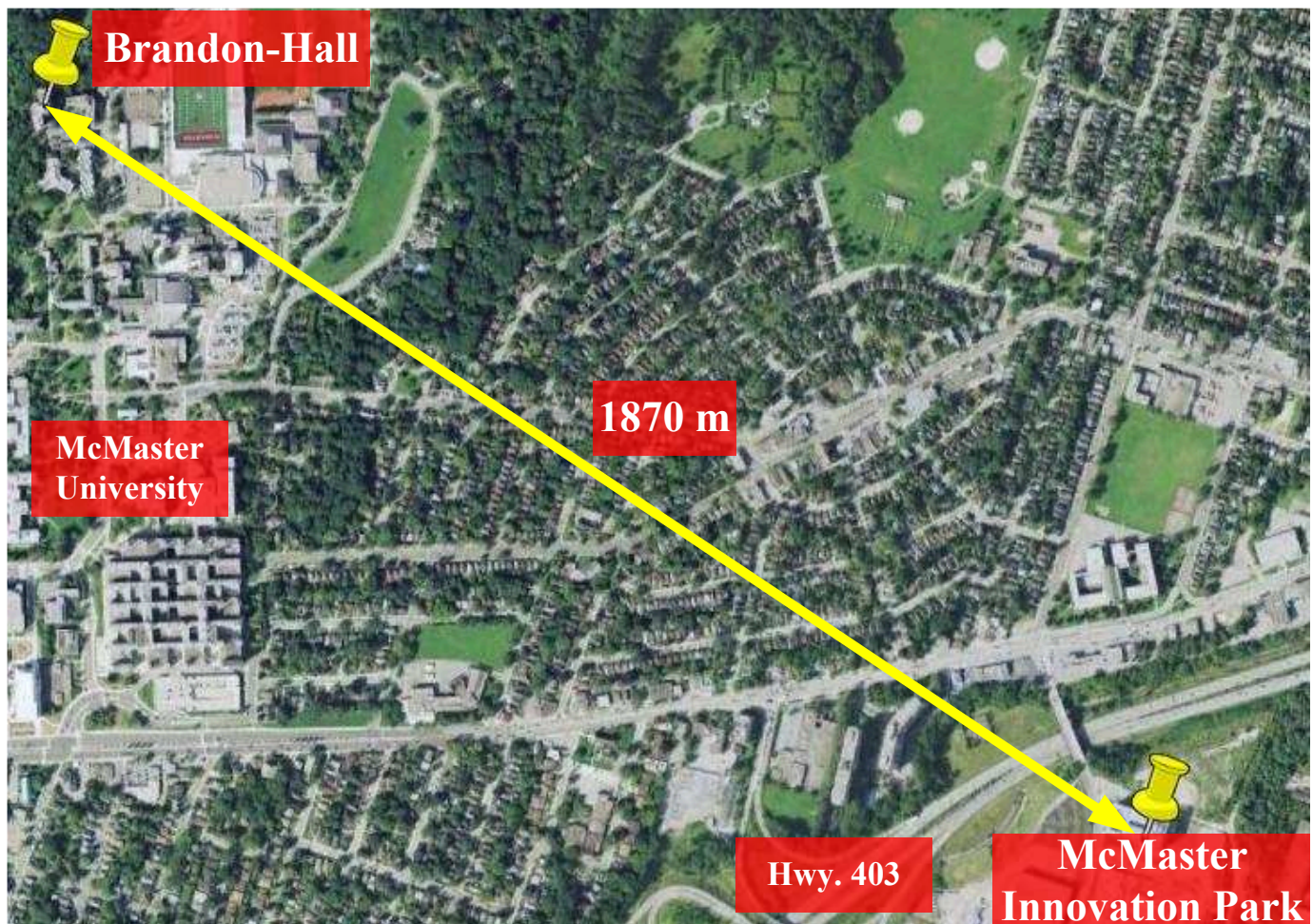
Fig. 1. Aerial view of the FSO link locations (**MIP** Lat.: 43° 15′ 23.75″ N, Long.: 79° 54′ 2.06″ W, **BH** Lat.: 43° 15′ 57.47″ N, Long.: 79° 55′ 10.99″ W) (satellite image ©2012 DigitalGlobe Inc. [11]).

A. FSO Terminals

The customized FSO terminals were deployed in August 2010 across McMaster University campus in west Hamilton area as illustrated in Fig. 1. One terminal is installed on the rooftop of the McMaster Innovation Park (MIP) building (approx. 21 m high) while the other terminal is installed on the rooftop of the Brandon Hall (BH) student residence (approx. 40 m high) at the north-west corner of McMaster University campus. The distance between the two terminals is approximately 1870 meters and the link passes over a major highway and many residential and commercial buildings.

1) Transmitters: Each terminal has four laser diodes at 1550 nm for transmission. Each laser has an independent driver and can operate at one of seven discrete power levels. The maximum radiated optical power of each laser is 60 mW after lenses and filters. The angle of divergence is 2.5 mrad full width at half maximum (FWHM). The optical head satisfies IEC Class-1M eye-safety standards. Only a single laser allows the analog transmission of an electrical signal provided by a standard 50-Ω, single-ended, AC-coupled SMB plug. Permitted input signal levels are ± 500 mV.

2) Receiver: The receiver aperture is 20 cm in diameter and has a 2.3-mrad field-of-view. Two spatial and two spectral solar filters are used to minimize the background and radiation noise. An avalanche photodiode (APD) receiver is used. The photodetector is followed by a transimpedance amplifier (TIA) with automatic gain control (AGC). For the experiments
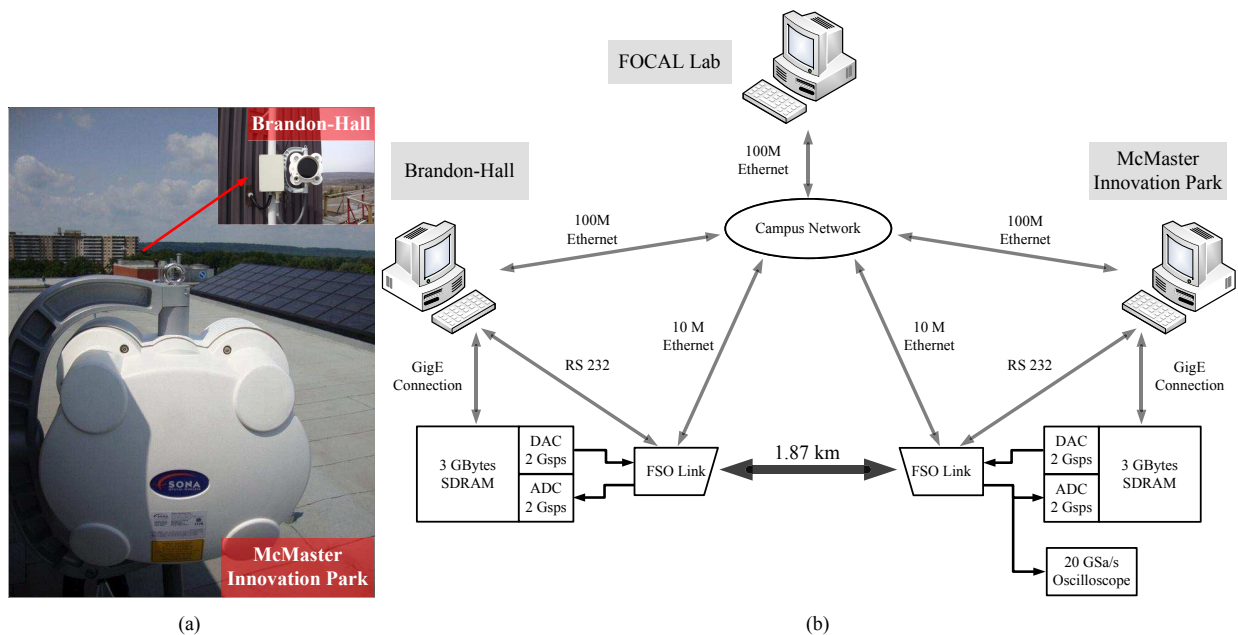
Fig. 2.   The experimental setup: (a) site-views, (b) block diagram.

reported here, the AGC is disabled and a fixed gain is set via control software. The output voltage is provided directly from the transimpedance amplifier operating in linear mode through a 100-Ω differential output via a pair of SMB connectors. Typical output levels are ± 30 mV at a TIA gain of 2000 V/A.

B. Digitizer Boards

The core processing units are three *Virtex*$^{\text{TM}}$-5 FPGAs from *Xilinx* [12]. Each FPGA is supported by two 512-MB DDR3 SDRAM memory banks, giving a total storage capacity of 3 GBytes on-board memory. The analog I/O front-end is supported by a 10-bit, 2-GSa/s ADC and a 12-bit, 2-GSa/s DAC output.

C. Experimental Setup

A block diagram of the entire experimental setup at both locations is shown in Fig. 2. Each FSO terminal is connected to a PC via an RS-232 port for control. For redundancy, each optical head has another connection to the McMaster University campus LAN via an Ethernet switch in case the roof PC fails. For data connections, each terminal is connected to a digitizer board where the DAC and ADC are connected to the FSO terminal analog transmitter and receiver, respectively. The digitizer board is connected to the PC via an optical Gigabit Ethernet link using an optical SFP to establish a UDP/IP connection for data transfer between the on-board memory and the PC as well as for controlling the board operation. The input to the ADC and DAC sampling clock is driven by an ultra low-noise 2-GHz crystal oscillator. A 4-channel, 20-GSa/s digital scope is used for visualizing signals. A weather station is fixed on top of the optical head at MIP. The weather station has software to log temperature, pressure, wind speed, wind direction, and rain level at 5-min intervals. The entire system at both locations is managed remotely from the FOCAL lab on campus.

III. TRANSCEIVER MEASUREMENT AND CHARACTERIZATION

This section presents measurement results to characterize the bandwidth and noise characteristics of the FSO link. The frequency response is used to ensure correct scaling of
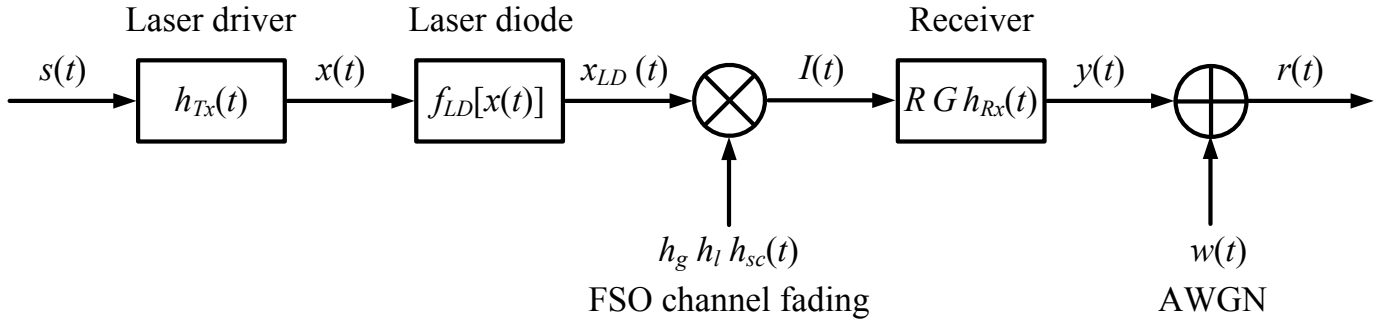
Fig. 3.   Proposed channel model for the FSO link.

measured fading. Characterization of the noise is necessary to permit future simulation of communication systems.

A. Channel Model

A proposed general channel model for the link is shown in Fig. 3. The received signal $r(t)$ can be expressed as

$$r(t) = R\,G\,h_g\,h_l\,h_{sc}(t)\,[f_{LD}\,[s(t) * h_{Tx}(t)] * h_{Rx}(t)] + w(t), \qquad (1)$$

where R is the photodetector responsivity, G is the transimpedance amplifier gain, h_g is the geometrical loss, h_l is the average atmospheric loss, $h_{sc}(t)$ is the scintillation, $f_{LD}(\cdot)$ is the laser transfer function taking non-linearity into consideration, $s(t)$ is the transmitted signal, $h_{Tx}(t)$ is the impulse responses of the laser driver, $h_{Rx}(t)$ is the impulse responses of the receiver, and $w(t)$ is an additive white Gaussian noise (AWGN). Laser non-linearity was measured and found to be negligible for the signal levels and frequencies used. Therefore, $f_{LD}\,[x(t)] \approx b\,x(t)$, where b is a constant that is assumed unity without loss of generality, and Eq. (1) can be rewritten as

$$r(t) = R\,G\,h_g\,h_l\,h_{sc}(t)\,[s(t) * h_{Tx}(t) * h_{Rx}(t)] + w(t),$$

which is simplified to

$$r(t) = h(t)\,[s(t) * h_{TxRx}(t)] + w(t), \qquad (2)$$

where $h(t) = R\,G\,h_g\,h_l\,h_{sc}(t)$ is the total channel gain and $h_{TxRx}(t) = h_{Tx}(t) * h_{Rx}(t)$ is the equivalent transceiver impulse response. In the following subsections, the frequency response, receiver noise, and optical power loss are experimentally quantified before presenting the channel measurements.

B. Frequency Response

The atmospheric channel itself has a very wide bandwidth. Frequency limitations arise mainly from the electronic components that make up the transmitter and receiver. The equivalent amplitude frequency response of the analog transmitter and receiver together, i.e. the magnitude of the Fourier transform of $h_{TxRx}(t)$ in (2), is obtained by estimating the power spectral density (PSD) of the received signal with a broadband input signal. To approximate such a signal, 101 equal amplitude sinusoids with frequencies from DC up to 1 GHz with 10 MHz step are transmitted simultaneously. The received waveform is sampled at 2 GSa/s. The resulting normalized PSD, shown in Fig. 4, is estimated using Welch's periodogram method [13]. Notice that the system acts as a low-pass channel with 3-dB cutoff frequency around 200 MHz.
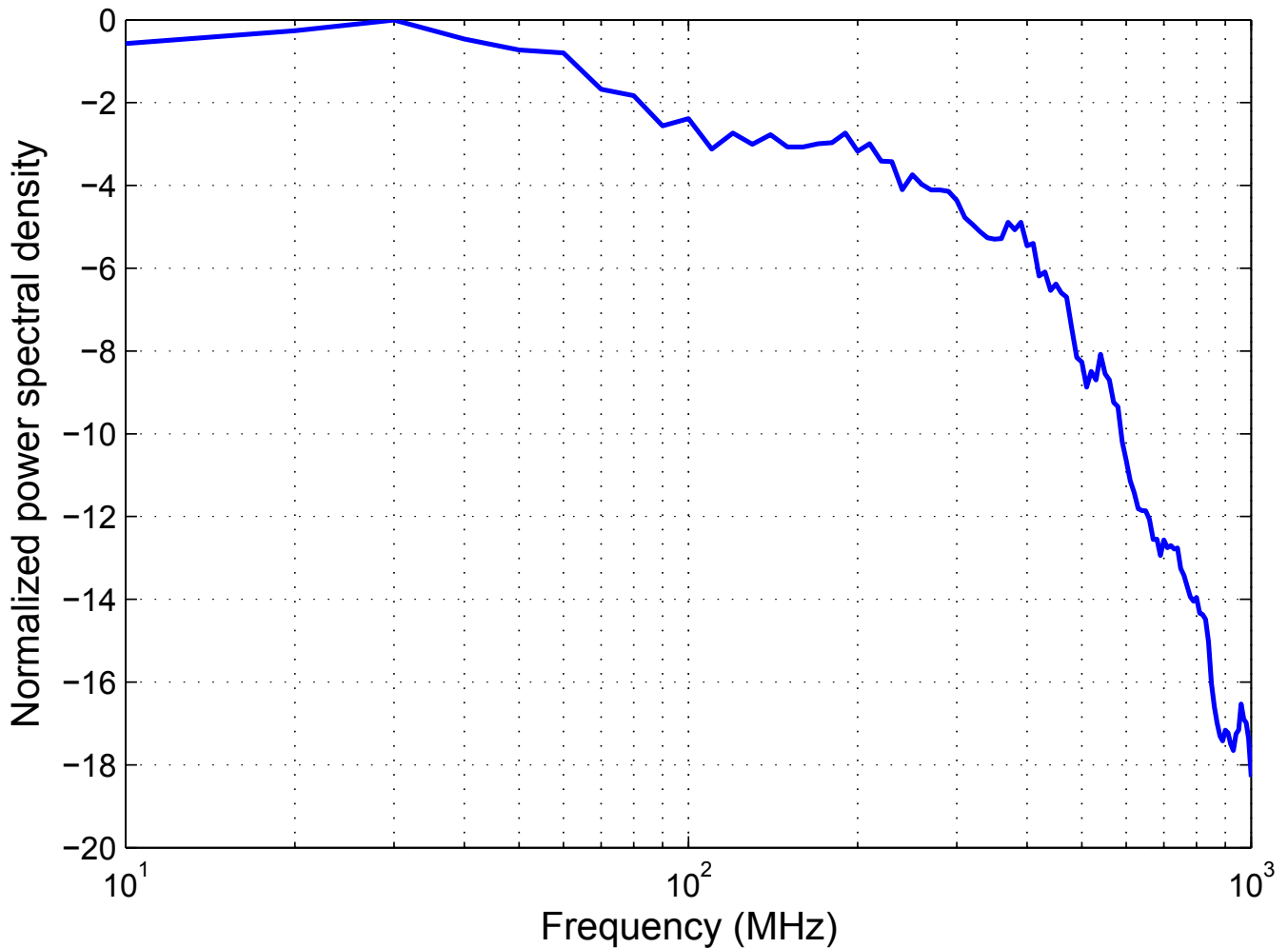
Fig. 4.   Normalized magnitude frequency response of the FSO link.

C. Noise

In FSO systems, the dominant noise sources are background radiation and circuit thermal noise at the receiver. Background and thermal noise is usually modelled as an additive and Gaussian distributed.

To obtain the noise statistics for the available setup, the laser transmitter is turned off and the receiver output is sampled at 2 GSa/s. Figure 5 shows the histogram of the noise samples, representing the background and thermal noise, along with the Gaussian fit using the maximum likelihood method [13].

The estimated mean and variance of the noise Gaussian distribution are given by $\mu_w = 0.62142$ mV and $\sigma_w^2 = 0.62906$ μV^2, respectively.

To quantify the effects of the background noise and thermal noise separately, the receiver aperture was covered to remove the background noise, however no difference in the noise statistics was observed. Also no difference was observed between day and night measurements. Therefore, noise at the receiver comes mainly from the thermal noise of the receiver electronics. The PSD of the noise was also investigated and showed that it has a first-null bandwidth in excess of 1 GHz. Thus, a reasonable model for the noise in the measurement system is AWGN.

$\mu = 0.62142$ mV
$\sigma = 0.79313$ mV
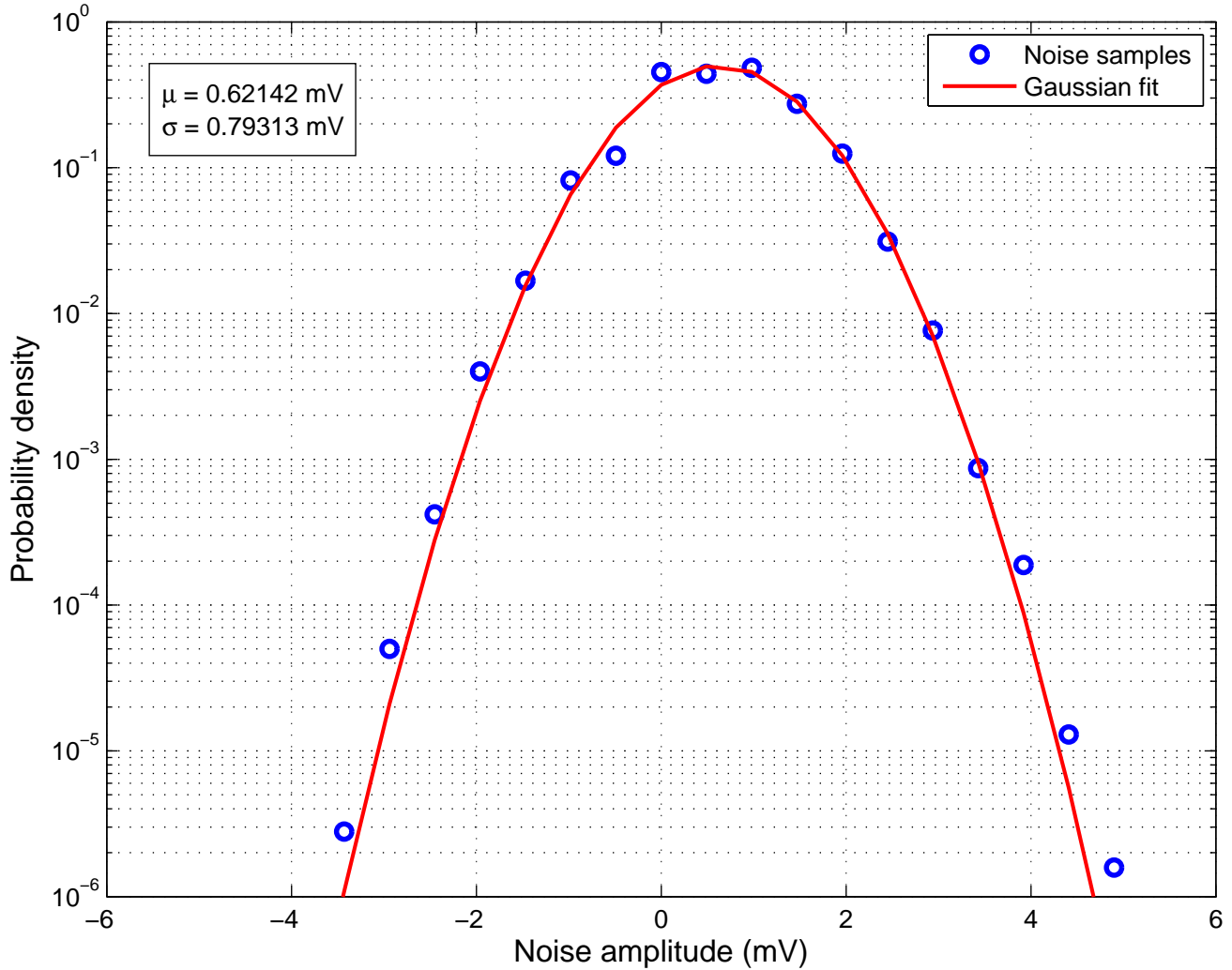
Fig. 5.   Thermal plus background noise samples at the receiver along with the Gaussian fit.

D. Power Loss Estimate

The maximum average optical power transmitted from the analog laser is 60 mW. At the receiver, the average received optical power for an unmodulated transmission in clear weather conditions (visibility is more than 24 km [14]) is 12 μW. Therefore, the average total loss in optical power at the receiver is approximately 37 dB. Out of many possible sources for the loss, propagation loss and the average atmospheric loss can be roughly estimated.

The propagation loss h_g can be estimated by [15]

$$h_g \approx \frac{D_{rx}^2}{(D_{tx} + \theta_{tx}L)^2} \approx \frac{D_{rx}^2}{(\theta_{tx}L)^2}, \qquad D_{tx} << \theta_{tx}L, \qquad (3)$$

where D_{tx} is the transmitting lens diameter, θ_{tx} is the transmitted beam divergence angle, L is the propagation distance, and D_{rx} is the receiving lens diameter. For the available FSO link, $\theta_{tx} = 2.5$ mrad, $L = 1.87$ km, and $D_{rx} = 0.2$ m. Therefore, the propagation loss is approximately 27 dB. In clear weather conditions, the average atmospheric loss is approximately 0.5 dB/km

[16]. Other possible sources of the power loss are alignment loss, receiver filters and lens loss, and coupling loss. Therefore, the total loss in the channel can be factored as

$$\underbrace{37 \text{ dB}}_{\text{Power loss}} = \underbrace{27 \text{ dB}}_{\substack{\text{Propagation loss} \\ h_g}} + \underbrace{1 \text{ dB}}_{\substack{\text{Atmospheric loss} \\ h_l}} + \underbrace{9 \text{ dB}}_{\substack{\text{Other} \\ \text{losses}}} .$$

IV. CHANNEL MEASUREMENTS AND DATA ANALYSIS

A. Measurement Procedure

Unlike previous work [17], [4], an optical intensity-modulated sinusoid is transmitted through the channel to measure the loss and fading, $h(t)$ in (2). At the receiver, an FFT is applied as a notch filter to the received samples to minimize the impact of noise corruption.

A block diagram of the signal processing system at the receiver is illustrated in Fig. 6. A sinusoid of frequency 117.187500 MHz is transmitted through the atmosphere from the analog laser. The received signal is sampled at 2 GSa/s and $8192 = 16 \times 512$ consecutive samples are buffered at a time. These samples are divided into 16 non-overlapping groups where each group undergoes a 512-point FFT implemented in an FPGA [18]. Notice that the transmit frequency is selected so that exactly 30 periods are applied to each 512-point FFT block. The following 11456 samples are discarded due to the latency in the FFT block.

For each FFT block, the real and imaginary coefficients corresponding to the bin containing the 117.187500-MHz frequency are selected to calculate the magnitude frequency response. Finally, the magnitudes of the 16 segments are averaged and buffered to the on-board memory with an 8-bit resolution. Bit growth during calculations is shown in Fig. 6 along the data path. Using the above measurement parameters produces channel samples at the rate of 101.8 kSa/s.

The FFT acts as a narrow band notch filter which rejects a large portion of the interfering noise. Measuring the spectral density of the received signal in clear weather shows that the average SNR is approximately 40 dB. The FFT bin width can be made narrow by increasing the length of the FFT at the expense of processing time and reduced sampling frequency. As a compromise between noise performance and FFT latency, the data samples are divided into 16 segments with parallel 512-FFT cores instead of a single 8192-FFT core. Such division reduces the overall latency by a similar factor of 16 allowing more samples to be processed.

B. Irradiance Fluctuations

Channel measurements using the technique described in Sec. IV-A have been collected during October and November 2011. The BH site was used as a transmitter while MIP was the receiver. The channel state h is captured at the rate 101.8 kSa/s at 8-bit resolution. Using all the available on-board memory (3 GBytes) permits continuous recording of the channel state for approximately 8 hours and 47 minutes. Then, a 24-min idle period is required to move the data from the board to a PC before capturing new samples.

1) Coherence Time: To gain insight into the channel behaviour during short time scales, consider Figures 7 (a), (b), (c), and (d) which plot the measured channel gain h during periods of 1 msec, 10 msec, 100 msec, and 1 sec, respectively.

The coherence time T_c measures the time duration wherein two received signals show high amplitude correlation. To estimate the FSO channel coherence time T_c, the autocovariance is calculated. The zero-mean channel gain $\tilde{h}$ is given as

$$\tilde{h} = h - \langle h \rangle = h - \frac{1}{N} \sum_{i=1}^{N} h_i, \tag{4}$$
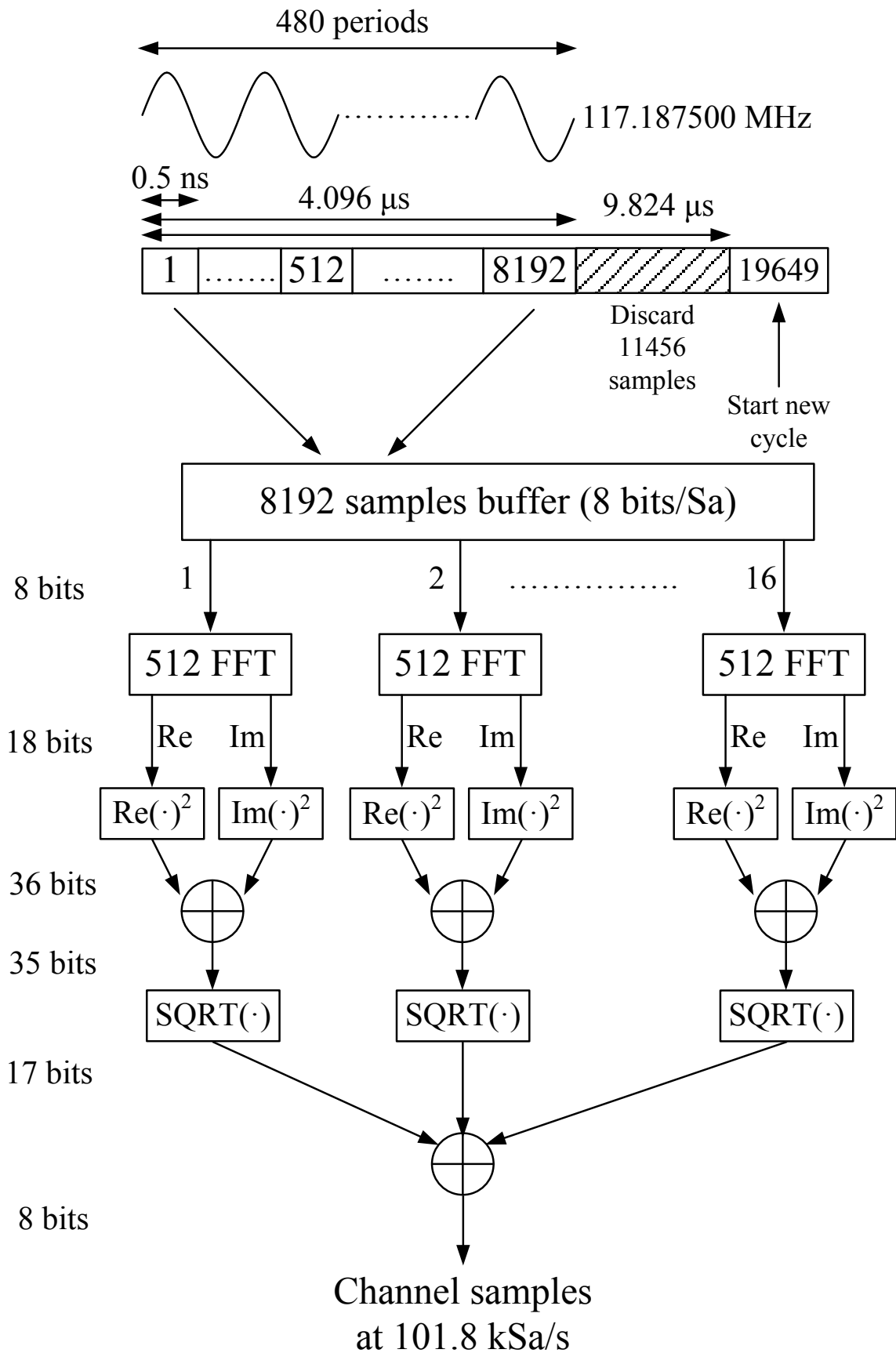
Fig. 6. Block diagram of the measurement system used at the receiver.
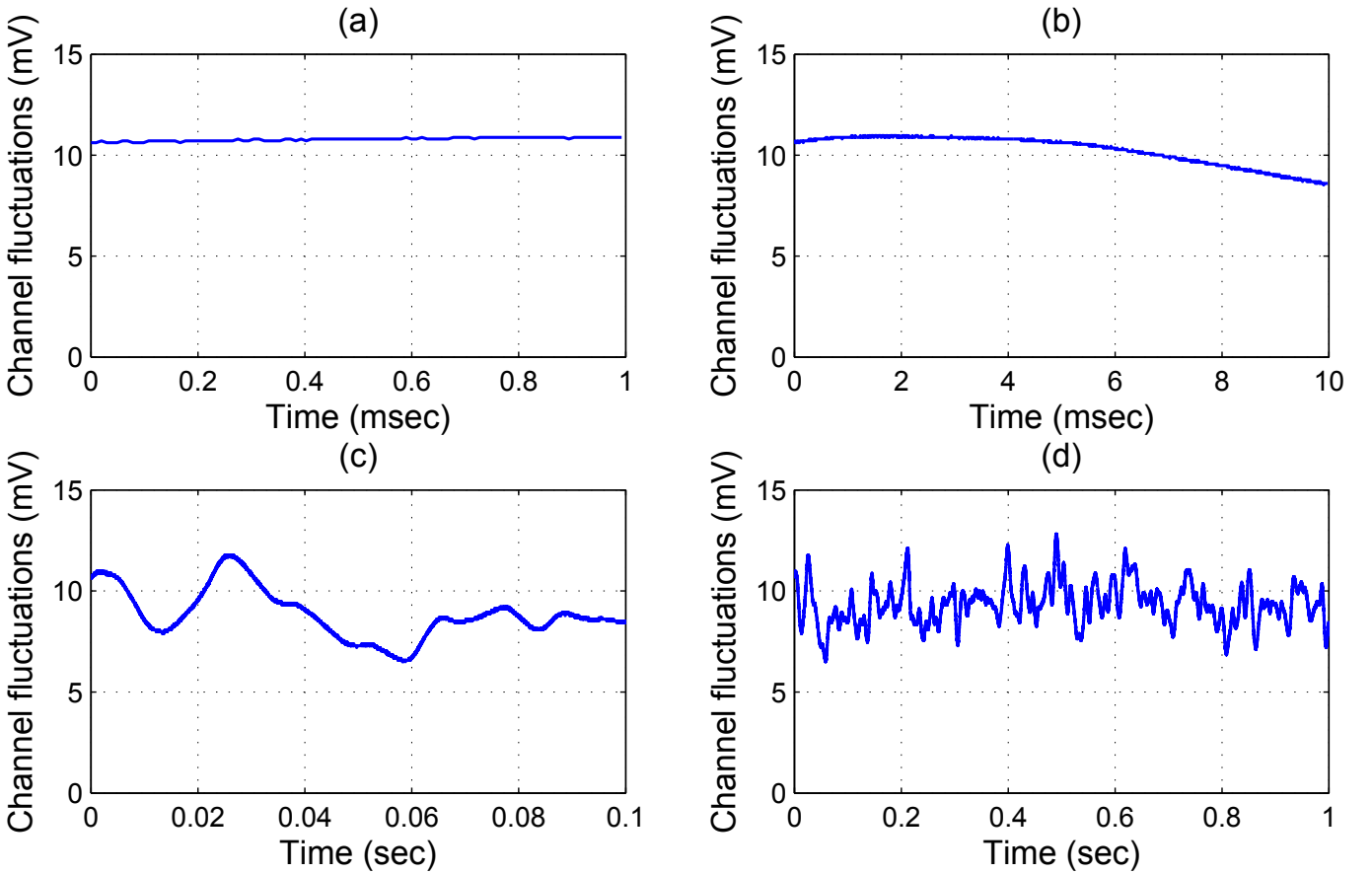
Fig. 7. Measured channel fluctuations at different time scales: (a) 1 msec, (b) 10 msec, (c) 100 msec, (d) 1 sec. (Oct. 30, 2011, 23:32 hrs, clear weather)

where h_i is the ith channel sample and N is the total number of samples used for the calculation. The autocovariance $R_{\tilde{h}\tilde{h}}$ is estimated by

$$R_{\tilde{h}\tilde{h}}(m) = \begin{cases} \sum_{n=1}^{N-m} \tilde{h}_{n+m}\tilde{h}_n & N-1 \geq m \geq 0 \\ R_{\tilde{h}\tilde{h}}(-m) & -N+1 \leq m < 0 \end{cases}. \tag{5}$$

The normalized autocovariance $\hat{R}_{\tilde{h}\tilde{h}}$ is obtained by

$$\hat{R}_{\tilde{h}\tilde{h}}(m) = \frac{R_{\tilde{h}\tilde{h}}(m)}{R_{\tilde{h}\tilde{h}}(0)}. \tag{6}$$

Figure 8 shows the normalized autocovariance computed via (6) from $N = 8$ MSa collected over 82.5 seconds on Oct. 31, 2011. The weather during this period of time is clear with temperature $7°$ C and wind speed 7.2 km/h. By considering the coherence time at $1/e$ of the peak at zero lag [19], i.e.

$$\hat{R}_{\tilde{h}\tilde{h}}(T_c) = 1/e, \tag{7}$$

the estimated coherence time $T_c \approx 6.5$ msec. Such coherence time justifies a slow-fading channel model for transmission rates in the megabit or gigabit per second ranges.

2) Scintillation Index: Scintillation index (SI) is the normalized variance of the irradiance fluctuations. For FSO channels, it is a measure of the optical turbulence strength that
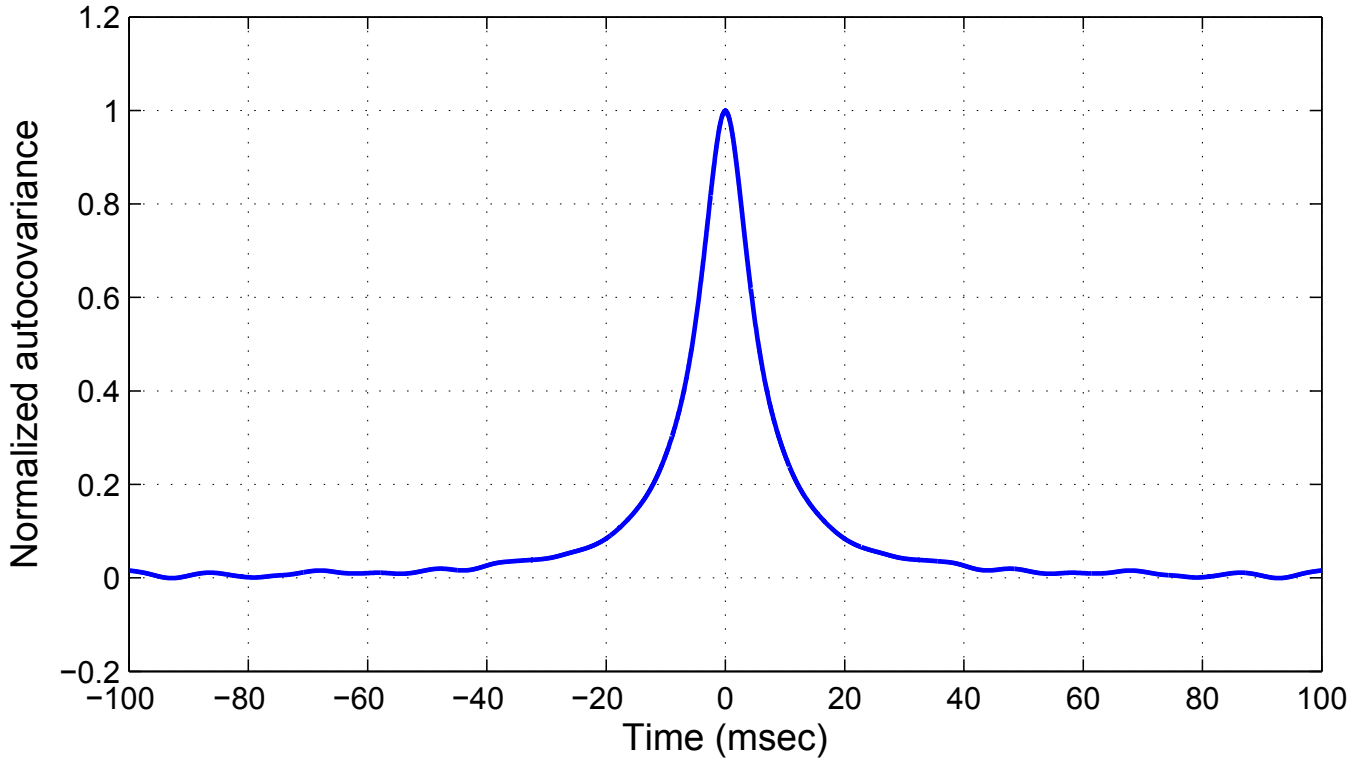
Fig. 8. Normalized autocovariance of the irradiance fluctuations. (Oct. 30, 2011, 23:32 hrs, clear weather)

causes random fluctuations of the received signal. The SI can be estimated from the channel measurements through

$$\mathrm{SI} = \frac{\langle h^2 \rangle - \langle h \rangle^2}{\langle h \rangle^2}, \tag{8}$$

where

$$\langle h^2 \rangle = \frac{1}{N} \sum_{i=1}^{N} (h_i - \langle h \rangle)^2 \qquad \text{and} \qquad \langle h \rangle = \frac{1}{N} \sum_{i=1}^{N} h_i,$$

where N is the number of measurements used in estimate.

For the sake of illustration, Figures 9 (a) and (b) show the average channel gain $\langle h \rangle$ (in mV) and the corresponding SI during a 14-hour period on Oct. 31, 2011 starting from midnight. Each measurement of SI or average gain is calculated using $N = 32$ MSa measurements, i.e., every 5.5 min.

Note that the gaps in the plots are the 24-min periods required to download the samples to the PC before a new collection of samples can be recorded. The average received value is relatively constant over the measurement period. Although the weather was clear, small changes are to be expected due to changes in wind speed, direction, pressure, as well as changing particulate density. Notice that at night (between 00:00 and 09:00 hrs), the temperature was in the range of $4-7°$ C and the wind speed was less than 2 km/h. Afterwards, the temperature increased to $11°$ C as did the wind speed between 8 and 16 km/h. In general, higher temperature and wind speeds correspond to stronger atmospheric turbulence and higher scintillation index.

C. Log-Normal, Gamma-Gamma, and Erlang Fitting

Many mathematical models for the FSO channel have been proposed since 1970s, however none of them can be universally applied due to the non-stationary nature of the atmospheric
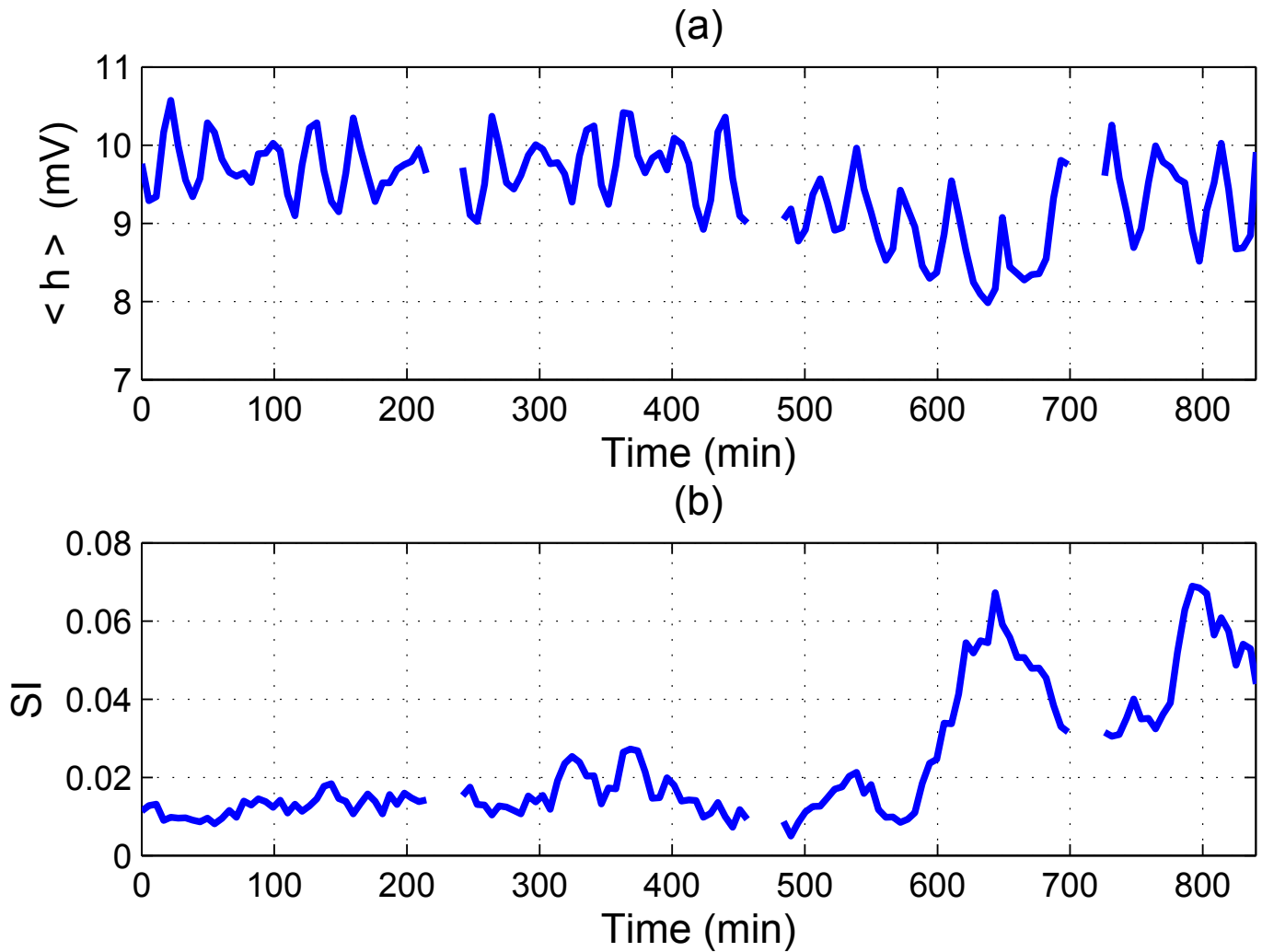
Fig. 9. Average intensity (a) and scintillation index (b) of the irradiance fluctuations during a 14-hour duration (Oct. 31, 2011, starting from 00:00 hrs until 14:00 hrs).

turbulence [1]. In this section, the measured channel gain is fit to some candidate distributions. As stated in the introduction, the aim of this work is to allow FSO communication designers to test the robustness of their algorithms directly using measured channel data, however, fitting to established distributions is useful to link with previous results.

In the weak-turbulence regime, the log-normal distribution is widely accepted because of the considerable match with the experimental measurements. Moreover, it is defined by a single-parameter making it mathematically tractable and permits obtaining closed-form expressions for error-rates. A log-normal distributed normalized fading channel (optical intensity) is described by [1]

$$p_{\hat{h},\mathrm{LN}}(\hat{h}) = \frac{1}{\sqrt{2\pi}\sigma_{\ln\hat{h}}\hat{h}} \exp\left(-\frac{\left(\ln\hat{h} + \frac{1}{2}\sigma_{\ln\hat{h}}^2\right)^2}{2\sigma_{\ln\hat{h}}^2}\right),$$

$$\hat{h} > 0, \qquad \langle\hat{h}\rangle = 1,$$

(9)

where $\sigma_{\ln\hat{h}}^2$ is the log-gain variance and $\hat{h}$ is the normalized channel samples given by $\hat{h} =$

$h/\langle h\rangle$. The scintillation index is calculated by

$$\mathrm{SI}_{\mathrm{LN}} = \exp\left(\sigma_{\ln\hat{h}}^2\right) - 1. \tag{10}$$

Under moderate-to-strong turbulence conditions, however, the log-normal distribution usually fails to give good fit with the measurements and doubly-stochastic distributions are applied [1]. The gamma-gamma distribution was proposed in [21] and has been shown to fit with the channel measurements under a wide range of atmospheric conditions. The PDF of a gamma-gamma distributed normalized channel fading $\hat{h}$ is given by [21]

$$p_{\hat{h},\mathrm{GG}}(\hat{h}) = \frac{2(\alpha\beta)^{\frac{\alpha+\beta}{2}}}{\Gamma(\alpha)\Gamma(\beta)}\hat{h}^{\frac{(\alpha+\beta)}{2}-1}K_{\alpha-\beta}(2\sqrt{\alpha\beta\hat{h}}),$$
$$\hat{h} > 0, \quad \langle\hat{h}\rangle = 1, \tag{11}$$

where $\Gamma(\cdot)$ is the gamma function, $K_v(\cdot)$ is the vth-order modified Bessel function of the second kind, and α and β are the effective parameters related to the large-scale and small-scale atmospheric fluctuations, respectively (refer to [21] for a detailed explanation). The scintillation index can be obtained from

$$\mathrm{SI}_{\mathrm{GG}} = \frac{1}{\alpha} + \frac{1}{\beta} + \frac{1}{\alpha\beta}. \tag{12}$$

Erlang distribution was suggested in [22] to model the atmospheric channel fading. The Erlang distribution is given by

$$p_{\hat{h},\mathrm{ER}}(\hat{h}) = \frac{\lambda^\theta}{(\theta-1)!}\hat{h}^{\theta-1}e^{-\lambda\hat{h}},$$
$$\hat{h} > 0, \quad \lambda > 0, \quad \theta \in \{1,2,3,...\}. \tag{13}$$

In this paper, we will consider fitting with these three distributions to link our channel measurements with previous work.

Fitting with the log-normal distribution (9) can be obtained using the maximum likelihood method [13] by finding $\bar{\sigma}_{\ln\hat{h}}^2$ that maximizes the log-likelihood function

$$\sum_{i=1}^{N}\ln\left\{\frac{1}{\sqrt{2\pi\sigma_{\ln\hat{h}}^2}\,\hat{h}_i}\exp\left(-\frac{\left(\ln\hat{h}_i + \frac{1}{2}\sigma_{\ln\hat{h}}^2\right)^2}{2\sigma_{\ln\hat{h}}^2}\right)\right\}.$$

The value of $\bar{\sigma}_{\ln\hat{h}}^2$ is given by

$$\bar{\sigma}_{\ln\hat{h}}^2 = \frac{1}{N}\sum_{i=1}^{N}\left(\ln\hat{h}_i - \frac{1}{N}\sum_{i=1}^{N}\ln\hat{h}_i\right)^2, \tag{14}$$

where $\hat{h}_i$ is the ith normalized channel sample. For the gamma-gamma distribution (11), the pair $\{\bar{\alpha},\bar{\beta}\}$ that maximizes the log-likelihood function can not be found analytically and numerical optimization techniques should be used. For Erlang distribution (13), estimating $\{\bar{\theta},\bar{\lambda}\}$ using the maximum likelihood method involves solving a mixed-integer optimization problem which is usually difficult to solve. Instead, $\{\bar{\theta},\bar{\lambda}\}$ can be found using a simple search algorithm. The integer parameter θ is substituted by $\theta^* = 1,2,3,......$ and the corresponding λ^* that maximizes the log-likelihood equation

$$\sum_{i=1}^{N}\ln\left\{\frac{\lambda^{\theta^*}}{(\theta^*-1)!}\hat{h}_i^{\theta^*-1}e^{-\lambda\hat{h}_i}\right\}$$

is calculated by

$$\lambda^* = \frac{N\theta^*}{\sum_{i=1}^{N}\hat{h}_i} = \theta^*.$$

Notice that $\langle\hat{h}\rangle = \frac{1}{N}\sum_{i=1}^{N}\hat{h}_i = 1$ for normalized channel samples. The value for θ^* is incremented until the maximum is obtained for the log-likelihood function where the required pair $\{\bar{\theta}, \bar{\lambda}\}$ is found.

Figures 10 and 11 show the histograms of the normalized channel samples $\hat{h}$ along with the log-normal, gamma-gamma, and Erlang fits in clear weather for large and small SI values, respectively. For both figures, the measurement duration is 165 sec (16 MSa). It can be seen from Fig. 10 that, for a relatively large SI value, the log-normal distribution deviates from the measurements histogram and fails to capture the tails at both small and large gain values. Notice that, in general, the gamma-gamma and Erlang distributions, give more accurate fits especially at low gains which are of greatest importance to communication designers. For the small SI value in Fig. 11, the three distributions are almost identical and show good fit with the measurements.

Figures 12 (a) and (b) show the channel in a rainy weather during a 1.29-sec and 165-sec measurement durations, respectively. It can be seen from the bump in Fig. 12 (b) that the channel statistics can vary considerably during rain due to changes in wind direction or rain rate. Thus, over the 165-sec duration the data is not a good fit to established fading models . However, a relatively better fit can be obtained for short durations as shown in Fig. 12 (a) for measurements during 1.29 sec using only 128 kSa. Thus, the data sets provide from this work capture the variation of channel gain in realistic changing rain environments allow for verification of FSO communication algorithms.

Although not reported here, during a heavy fog condition, on Nov. 8, 2011 at 8:50 PM, the visibility was less than 200 m and no optical power was received and all the obtained samples were zero.

It should be noted that all the obtained SI values are relatively small. Even in very hot days during July, SI never exceeded 0.15. Such reduced SI can be related to the relatively large area of the receiver that alleviates the effect of the atmospheric turbulence on the received signal due to the aperture-averaging effect [3].

V. MARKOV MODELLING

A finite-state Markov chain can be directly applied to model the time-varying behaviour of discrete fading communication channels [23], [24], [25], [26]. The main idea is to divide the set of channel measurements into a finite number of discrete levels which are mapped to states. The transitions between states are then estimated using the measured data to yield a homogeneous Markov chain representation of the fading process.

Let $\mathcal{S} = \{s_0, s_1, s_2, ..., s_{K-1}\}$ denote a finite set of K states and let S_n denote the state of Markov process at time step n. The process $\{S_n\}$ is assumed to be stationary in time. To link the measured fading value h to the states, consider partitioning the set of received amplitudes into K uniform intervals of size

$$\Delta = \frac{h_{\max} - h_{\min}}{K}, \tag{15}$$

where $h_{\max}$ and $h_{\min}$ denote the maximum and minimum received measurements in the data set, respectively. At time step n, the measured channel value is h_n and the state of Markov chain is $S_n = s_k$, where k is selected so that

$$h_{\min} + k\Delta \leq h < h_{\min} + (k+1)\Delta \tag{16}$$
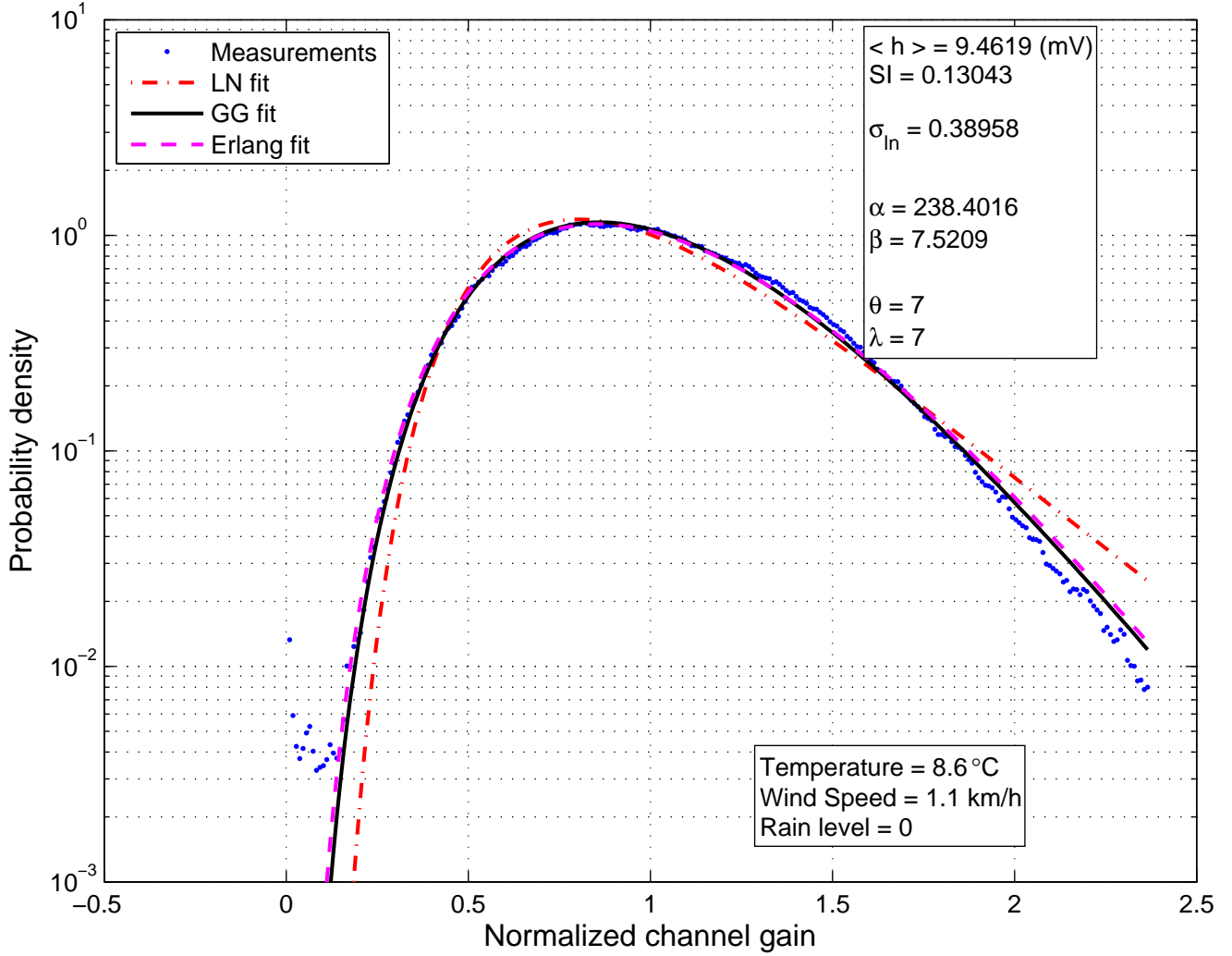
Fig. 10. Histogram of normalized channel gain, $\hat{h}$, under large scintillation index condition along with log-normal $\{\sigma_{\ln}\}$, gamma-gamma $\{\alpha, \beta\}$, and Erlang $\{\theta, \lambda\}$ fits in clear weather conditions (samples measured on Nov. 1, 2011 at 11:07 PM).

for $k \in \{0, 1, 2, ..., K - 1\}$. For each state s_k, a representative output amplitude is assigned as $h^{(k)} = h_{\min} + (k + 1/2)\Delta$.

Let $\mathbf{T} = [t_{j,k}]_{K \times K}$ denote the state transition matrix of the Markov process. For a sufficiently large total number channel measurements N, the elements of $\mathbf{T}$ can be estimated as

$$t_{j,k} = \Pr(S_{n+1} = s_k | S_n = s_j) = \frac{N_{j,k}}{\sum_{l=0}^{K-1} N_{l,j}} = \frac{N_{j,k}}{N_j},$$
$$j, k \in \{0, 1, 2, ..., K - 1\}, \tag{17}$$

where $N_{j,k}$ is the number of observed transitions from state s_j to state s_k and N_j is the total number of times the channel measurement was at state s_j.

For the sake of illustration, a group of $N = 2^{24}$ channel samples obtained during a 165-sec measurement period with sampling rate 101.8 kSa/s are used to derive the Markov model. These samples were measured on Oct. 30, 2011 at 11:32 PM during clear weather (the same data set used to generate Figures 7 and 8). The full range of the samples ($h_{\min} =$
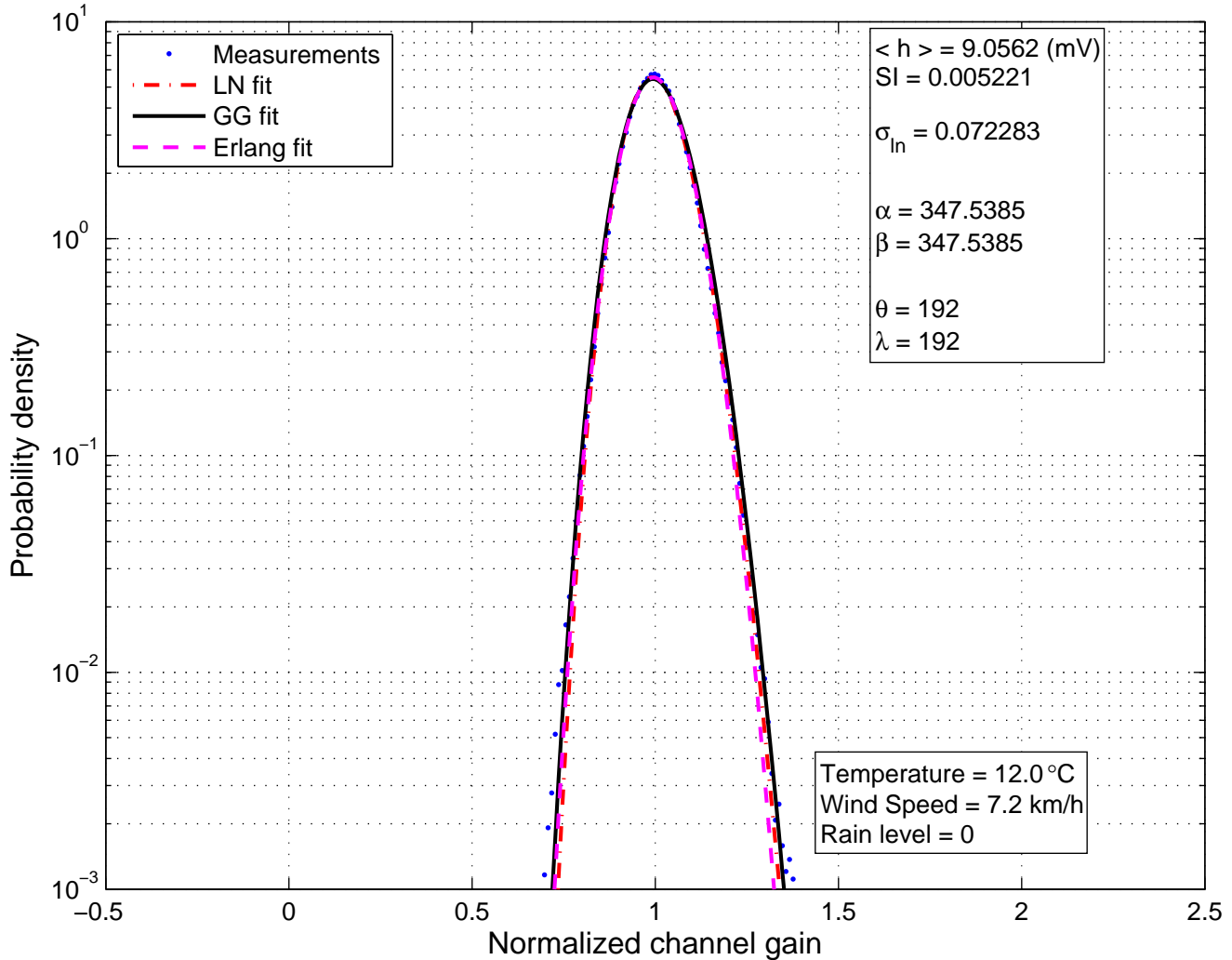
Fig. 11. Histogram of normalized channel gain, $\hat{h}$, under small scintillation index along with log-normal $\{\sigma_{\ln}\}$, gamma-gamma $\{\alpha, \beta\}$, and Erlang $\{\theta, \lambda\}$ fits in clear weather conditions (samples measured on Nov. 2, 2011 at 09:18 AM).

5.35 mV, $h_{\max} = 15.36$ mV) is divided uniformly into $K = 8$ partitions. The entries of **T**, obtained using (17), are shown in Table I.

It can be seen from Table I that, for any state, the probability of transition $t_{j,k}, \ j \neq k$, is always less than the self-loop probability $t_{j,j}$, which is higher than 96%, due to the slow-varying nature of the channel. Also these transitions only occur between adjacent states, i.e. $t_{j,k} = 0, \ \forall |j-k| > 1$, which is a typical property of finite-state Markov models for slow-fading channels [23].

Note that the above steps can be taken for any number of states K. In order to see the impact of K on the model, the steps were repeated for $K = 64$, however, the transition matrix is not reported here due to its large size and can be found online [8].

Figure 13 shows the histograms of the measured channel samples and the samples generated by the Markov models. The good match with the resulting channel distributions is noticed. Table II shows the average channel gain, scintillation index, and coherence time, defined by (7), obtained from the measurements and simulation. Figure 14 shows the ability of the Markov model to generate channel samples with autocovariance that fits well with the
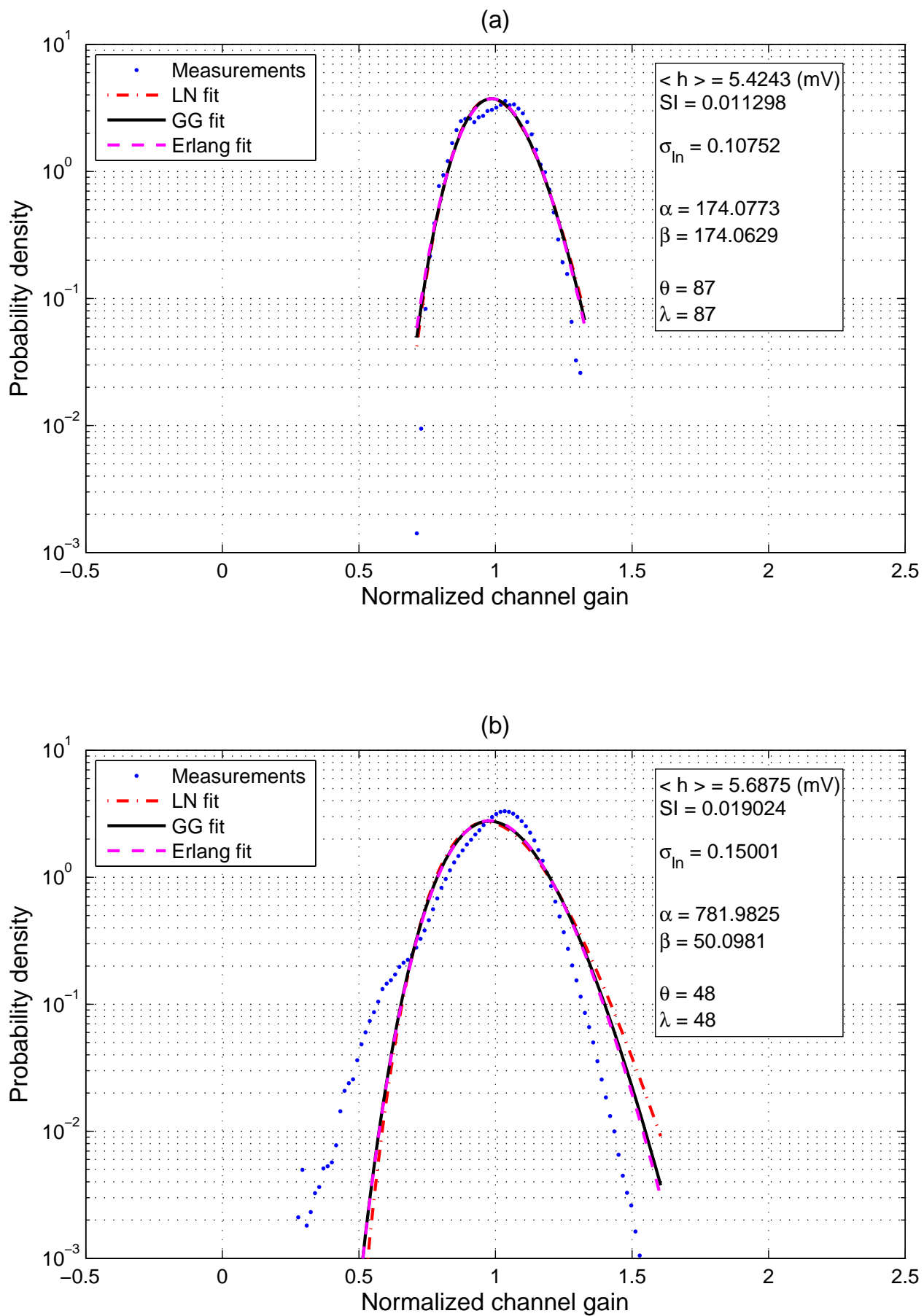
Fig. 12. Histogram of normalized channel gain, $\hat{h}$, along with log-normal $\{\sigma_{\ln}\}$, gamma-gamma $\{\alpha, \beta\}$, and Erlang $\{\theta, \lambda\}$ fits in light rain condition (temperature: 1.9 °C, wind speed: 24.46 km/hr, rain level: 0.9 mm/hr) during two measurement

TABLE I
STATE-TRANSITION PROBABILITY MATRIX OF THE MARKOV CHAIN MODEL WHEN $K = 8$.

	$k = 0$	$k = 1$	$k = 2$	$k = 3$	$k = 4$	$k = 5$	$k = 6$	$k = 7$
$j = 0$	0.9617	0.0383	0	0	0	0	0	0
$j = 1$	0.0016	0.9727	0.0257	0	0	0	0	0
$j = 2$	0	0.0038	0.9813	0.0149	0	0	0	0
$j = 3$	0	0	0.0097	0.9841	0.0062	0	0	0
$j = 4$	0	0	0	0.0205	0.9757	0.0037	0	0
$j = 5$	0	0	0	0	0.0274	0.9694	0.0032	0
$j = 6$	0	0	0	0	0	0.0301	0.9678	0.0021
$j = 7$	0	0	0	0	0	0	0.0292	0.9708

TABLE II
COMPARISON BETWEEN MEASUREMENTS AND THE MARKOV MODEL.

	Experimental	Markov $(K = 64)$	Markov $(K = 8)$
$\langle h \rangle$	9.4612 mV	9.4464 mV	9.4557 mV
SI	0.0113	0.0116	0.0123
T_c	6.5 msec	5.6 msec	0.74 msec

autocovariance of the measured channel samples when $K = 64$, however, the fit is loose for $K = 8$. The comparison justifies that the obtained Markov model gives a good approximation to the channel behaviour and can be used for generating channel realizations for simulation purposes. The Markov model is simple and computationally-efficient since it is completely defined by the sparse matrix T. Such a model can be used to accurately generate different FSO channel realizations with correct distribution and autocorrelation.

VI. CONCLUSIONS

This paper presents measurement results and channel modelling of an urban FSO channel. Unlike earlier work, we employ modified commercial transceivers and have collected a library of channel measurements in clear and light rain weather conditions. Thus, all of the trade-offs inherent in the design of a commercial FSO product are reflected in our measurements. The measurement system was implemented on a high-speed FPGA board where FFT cores were used to achieve measurement SNRs of approximately 40 dB. Fitting to the log-normal, gamma-gamma, and Erlang distributions and measurements of the coherence time in clear weather are also presented. The channel gain is measured in light rain and clear weather conditions and a complete library of these measurements is available for download [8]. We intend to post new channel measurements to this database on a continuing basis under a greater variety of weather conditions. It is our sincere hope that this data set will aid FSO communication system designers to evaluate the performance of their algorithms using realistic channel data.

A finite-state Markov chain model is derived from the channel measurements and shown to model both the distribution and autocorrelation properties of the turbulence-induced fading. In particular the 64-state model showed good agreement and is also available for download [8].

The developed channel measurement system will be run continuously throughout the year to produce a large database of channel measurements under different weather conditions. Such a database will be used to build comprehensive statistical models and empirical formulas that directly relate the weather parameters with the channel statistics and the performance of the communication link.
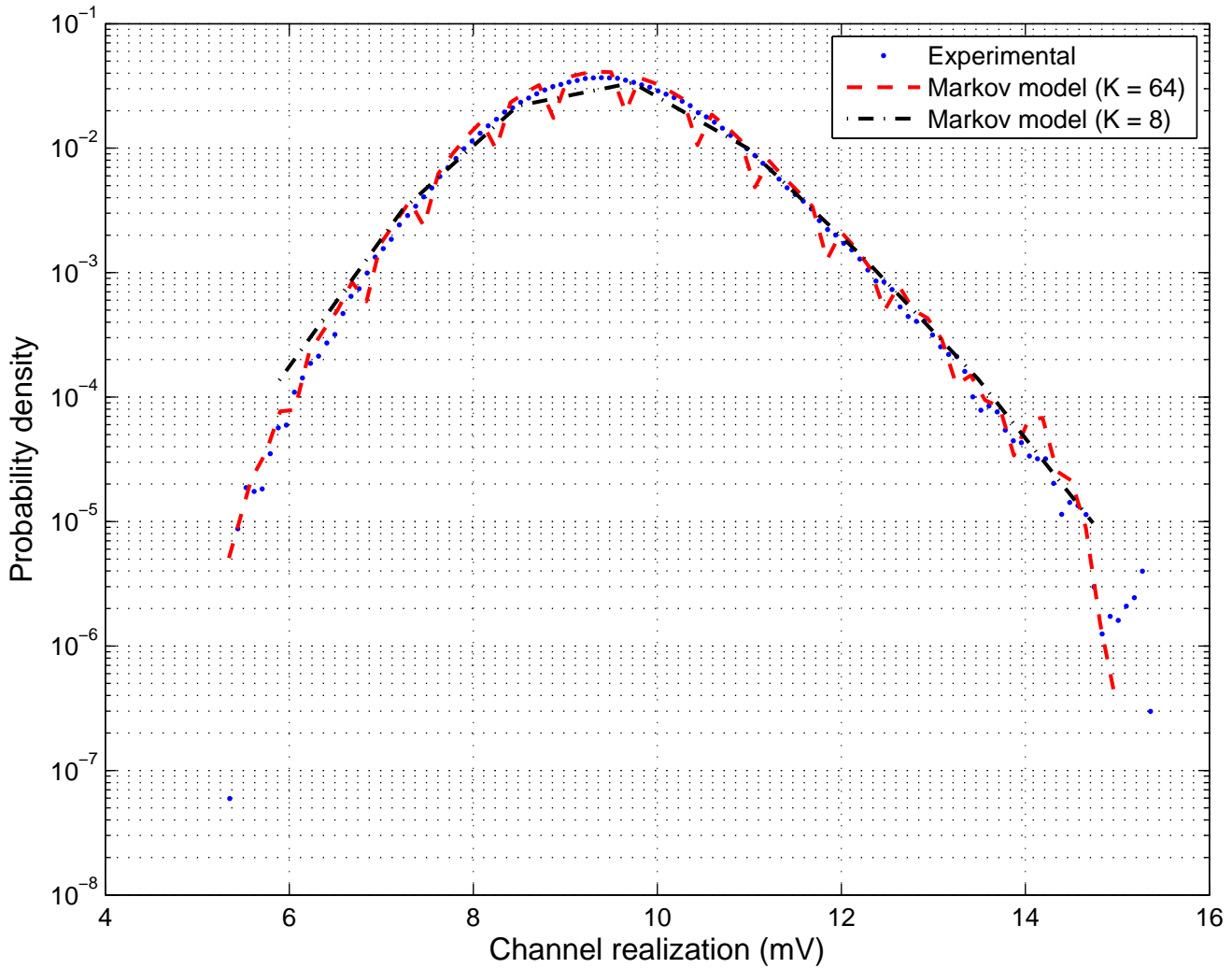
Fig. 13. The histograms of the channel realizations obtained from the measurements and the realizations generated by the Markov model (samples measured on Oct. 30, 2011, 23:32 hrs, clear weather).

REFERENCES

[1] L. C. Andrews and R. L. Phillips, *Laser Beam Propagation through Random Media*, 2nd ed. Bellingham, Washington: SPIE, 2005.

[2] M. E. Gracheva and A. S. Gurvich, "Strong fluctuations in the intensity of light propagated through the atmosphere close to the earth," *Radiofiz.*, vol. 8, no. 4, pp. 717–724, 1965.

[3] F. S. Vetelino, C. Young, L. Andrews, and J. Recolons, "Aperture averaging effects on the probability density of irradiance fluctuations in moderate-to-strong turbulence and spherical waves in the atmosphere," *Journal of Applied Optics*, vol. 46, no. 11, pp. 2099–2108, April 2007.

[4] A. Khatoon, W. G. Cowley, and N. Letzepis, "Channel measurement and estimation for free space optical communications," in *AusCTW 2011*, January - February 2011.

[5] F. S. Marzano, S. Mori, F. Frezza, P. Nocito, G. M. T. Beleffi, G. Incerti, E. Restuccia, and F. Consalvi, "Free-space optical high-speed link in the urban area of southern Rome: preliminary experimental set up and channel modelling," in *Proceedings of the 5th European Conference on Antennas and Propagation (EUCAP)*, April 2011, pp. 2737 – 2741.

[6] K.-H. Kim, T. Higashino, K. Tsukamoto, and S. Komaki, "Optical fading analysis considering spectrum of optical scintillation in terrestrial free-space optical channel," in *International Conference on Space Optical Systems and Applications*, Santa Monica, CA, May 2011, pp. 58–66.

[7] M. Gebhart, E. Leitgeb, and J. Bregenzer, "Atmospheric effects on optical wireless links," in *Proceedings of the 7th International Conference on Telecommunications, ConTEL 2003*, vol. 2, Zagreb, Croatia, June 2003, pp. 395 – 401.
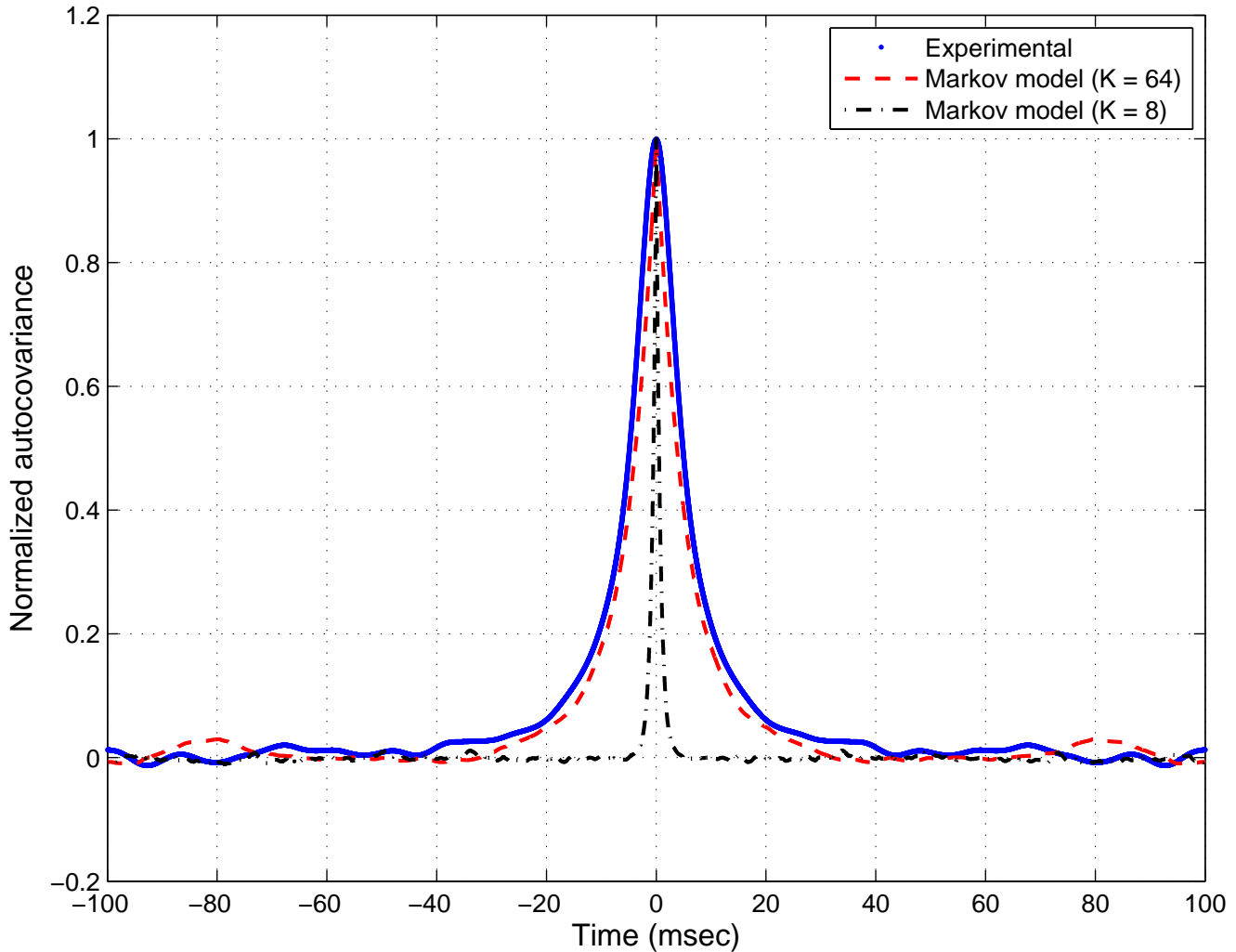
Fig. 14.   Normalized autocovariance of the channel realizations obtained from the measurements and generated by the Markov model.

[8] "Free-Space Optical Communication Algorithms Laboratory (FOCAL), McMaster University." [Online]. Available: focal.mcmaster.ca

[9] *fSONA* Networks, Inc. (2011) *fSONA*: free Space Optical Networking Architecture. [Online]. Available: http://www.fsona.com/

[10] TEK Microsystems, Inc., "TekMicro." [Online]. Available: http://www.tekmicro.com/

[11] DigitalGlobe, Inc. (2012) Satellite Imagery and Geospatial Information Products. [Online]. Available: http://www.digitalglobe.com/

[12] Xilinx, Inc. (2011). [Online]. Available: http://www.xilinx.com/support/documentation/virtex-5.htm

[13] S. M. Kay, *Modern Spectral Estimation: Theory And Application*.   Prentice Hall, Englewood Cliffs, New Jersey, 1988.

[14] "The weather network." [Online]. Available: http://www.theweathernetwork.com/weather/caon0289

[15] H. Willebrand and B. S. Ghuman, *Free Space Optics: Enabling Optical Connectivity in Today's Networks*.   Sams Publishing, 2002.

[16] I. Kim, J. Koontz, H. Hakakha, P. Adhikari, R. Stieger, C. Moursund, M. Bar-clay, A. Stanford, R. Ruigrok, J. Schuster, and E. Korevaar, "Measurement of scintillation and link margin for the terralink laser communication system," *Proceedings of the SPIE*, pp. 100–118, January 1998.

[17] F. S. Vetelino, B. Clare, K. Corbett, C. Young, K. Grant, and L. Andrews, "Characterizing the propagation path in moderate to strong optical turbulence," *Journal of Applied Optics*, vol. 45, no. 15, pp. 3534–3543, May 2006.

[18] "Xilinx LogiCORE IP Fast Fourier Transform v7.1," March 2011. [Online]. Available: http://www.xilinx.com/support/documentation/ip_documentation/xfft_ds260.pdf

[19] G. R. Osche, *Optical detection theory for laser applications*. Wiley-Interscience, 2002.

[20] "NIST/SEMATECH e-handbook of statistical methods." [Online]. Available: http://www.itl.nist.gov/div898/handbook/

[21] M. A. Al-Habash, L. C. Andrews, and R. L. Phillips, "Mathematical model for the irradiance probability density function of a laser beam propagating through turbulent media," *Optical Engineering*, vol. 40, pp. 1554–1562, August 2001.

[22] M. L. B. Riediger, R. Schober, and L. Lampe, "Multiple-symbol detection for photon-counting MIMO free-space optical communications," *IEEE Transactions on Wireless Communications*, vol. 7, no. 12, pp. 5369–5379, December 2008.

[23] H. S. Wang and N. Moayeri, "Finite-state Markov channel - a useful model for radio communication channels," *IEEE Transactions on Vehicular Technology*, vol. 44, no. 1, pp. 163–171, February 1995.

[24] Q. Zhang and S. Kassam, "Finite-state Markov model for Rayleigh fading channels," *IEEE Transactions on Communications*, vol. 47, no. 11, pp. 1688–1692, November 1999.

[25] V. Bhaskar, "Finite-state Markov model for lognormal, chi-square (central), chi-square (non-central), and K-distributions," *International Journal of Wireless Information Networks*, vol. 14, no. 4, pp. 237–250, October 2007.

[26] X. Zhu and J. M. Kahn, "Markov chain model in maximum-likelihood sequence detection for free-space optical communication through atmospheric turbulence channels," *IEEE Transactions on Communications*, vol. 51, no. 3, pp. 509–516, March 2003.

PLACE
PHOTO
HERE

Ayman Mostafa (S'08) received the B.Sc. degree with honours in electrical engineering from Alexandria University, Egypt in 2006 and the M.A.Sc. degree in electrical engineering from McMaster University, Canada in 2012.

He is currently working toward the Ph.D. degree in electrical engineering at the University of British Columbia, Canada.

His current research interests are in RF propagation, channel modelling, and distributed MIMO systems.

PLACE
PHOTO
HERE

Steve Hranilovic (S'94-M'03-SM'07) received the B.A.Sc. degree with honours in electrical engineering from the University of Waterloo, Canada in 1997 and M.A.Sc. and Ph.D. degrees in electrical engineering from the University of Toronto, Canada in 1999 and 2003 respectively.

He is currently an Associate Professor in the Department of Electrical and Computer Engineering, McMaster University, Hamilton, Ontario, Canada. During 2010-2011 he spent his research leave as Senior Member, Technical Staff in Advanced Technology for Research in Motion, Waterloo, Canada. His research interests are in the areas of free-space and wired optical communications, digital communication algorithms, and electronic and photonic implementation of coding and communication algorithms. He is the author of the book *Wireless Optical Communications Systems* (New York:Springer, 2004).

Dr. Hranilovic is a licensed Professional Engineer in the Province of Ontario and was awarded the Government of Ontario *Early Researcher Award* in 2006. He currently serves as an Associate Editor for the *IEEE Transactions on Communications* in the area of Optical Wireless Communications.